# Evolution of indium segregation in metal-polar $In_{0.17}Al_{0.83}N$ lattice-matched to GaN grown by plasma assisted molecular beam epitaxy

A. Senichev[a,b], T. Nguyen[b], R.E. Diaz[a], B. Dzuba[b], M. Shirazi-HD[a,c], Y. Cao[b], M.J. Manfra[a,b,c,d], O. Malis[b,*]

[a] Birck Nanotechnology Center, West Lafayette, IN 47907, USA
[b] Department of Physics and Astronomy, Purdue University, West Lafayette, IN 47907, USA
[c] School of Electrical and Computer Engineering, Purdue University, West Lafayette, IN 47907, USA
[d] School of Materials Engineering, Purdue University, West Lafayette, IN 47907, USA

ABSTRACT

The impact of growth conditions on indium segregation in metal-polar $In_{0.17}Al_{0.83}N$ lattice-matched to GaN grown by plasma assisted molecular beam epitaxy is reported. A series of lattice-matched InAlN films was systematically grown over a wide range of temperatures and active nitrogen fluxes. The growth conditions include those reported in the literature as conducive to homogeneous $In_{0.17}Al_{0.83}N$ (Kaun et al., 2014). However, honeycomb indium composition modulation was found in all InAlN films. For samples grown at the highest temperature and nitrogen flux, InAlN layers exhibit larger and more irregular cells with emergence of open cell boundaries. We conclude that the studied growth conditions alone are not sufficient to eliminate the 'honeycomb' structure in metal-polar InAlN lattice-matched to GaN, and that the physical process necessary for reproducible growth of homogeneous $In_{0.17}Al_{0.83}N$ requires further clarification.

$In_xAl_{1-x}N$ with indium composition of $x \sim 0.17$ is an attractive material for nearly strain-free electronic and photonic devices because it has the same in-plane lattice constant as c-plane GaN. The strong difference in spontaneous polarization between InAlN and GaN provides a high sheet carrier charge density in two-dimensional electron gases (2DEG) in high electron mobility transistors (HEMTs) [2]. Additionally, lattice-matched $In_{0.17}Al_{0.83}N$/GaN can eliminate the high-voltage induced formation of defects in HEMTs through the inverse piezoelectric effect, which is particularly important for high-power, high-frequency electronics [3]. Advantages of lattice-matched InAlN/GaN systems were already demonstrated for HEMTs with a record current gain cutoff frequency of 300 GHz [4], light-emitting diodes with an improved internal quantum efficiency using InAlN electron-blocking layers [5,6], and superlattices with enhanced near-infrared intersubband absorption [7,8].

Growth of homogeneous metal-polar $In_{0.17}Al_{0.83}N$ by plasma-assisted molecular beam epitaxy (PAMBE) remains challenging. InAlN is subject to segregation into In-rich regions and Al-rich regions that deviate from the expected random alloy distribution. Due to strong differences between its constituent binaries, AlN and InN, InAlN often displays a 'honeycomb' microstructure [9–11]. In work by Sahonta et al. [9], the growth of InAlN films by PAMBE is described as a three

step process: formation of Al-rich InAlN dynamical platelets, partial coalescence, and then preferential indium incorporation at platelet boundaries due to tensile strain generated between platelets. Thus, the growth process includes a quasi-three-dimensional stage at the onset of InAlN nucleation on GaN and then a transition to further two-dimensional growth, which was also observed during the growth of InN at low temperatures [12]. To our knowledge, only one group has reported elimination of the 'honeycomb' microstructure in metal-polar $In_{0.17}Al_{0.83}N$ films supported with extensive analysis of indium distribution [1]. In Ref. [1], homogeneous lattice-matched $In_{0.17}Al_{0.83}N$ layers were achieved by PAMBE in the nitrogen-rich regime by increasing indium to aluminum ratio and the growth temperature as compared to earlier work from the same group in which InAlN films with an inhomogeneous indium distribution were reported [10]. However, the growth processes responsible for driving the transition from an inhomogeneous to homogeneous alloy were not discussed. The goal of this work is to elucidate the growth dynamics of InAlN lattice-matched to GaN by probing a wide range of growth conditions.

We study the impact of growth conditions on indium segregation in metal-polar InAlN alloys grown by PAMBE. In particular, we focus on InAlN with the technologically important indium mole fraction $x \sim 0.17$ that is lattice-matched to GaN. A series of nearly lattice-matched InAlN/

GaN samples was grown while systematically varying the nitrogen flux, substrate temperature, and indium flux to preserve the lattice-matched condition. From this data we construct a growth diagram for $In_{0.17}Al_{0.83}N$ lattice-matched to GaN over a wide range of conditions. Importantly, our explored growth parameters include those reported for homogeneous lattice-matched InAlN/GaN [1]. In our experimental approach, the indium composition at a given nitrogen flux was controlled by substrate temperature. The impinging indium flux was always selected large enough to ensure a saturated (maximum) indium mole fraction, and steady-state growth with excess indium on the surface as evidenced by sparse indium droplets on the surface at the termination of growth. This corresponds to growth under an indium adlayer, while still in the nominally nitrogen-rich growth regime in terms of impinging fluxes. The formation of an indium adlayer is also facilitated by InN decomposition at the growth temperatures explored here. We observe a gradual evolution of the honeycomb microstructure with growth conditions. The cell size increases with substrate temperature and nitrogen flux. For samples grown at the highest temperature and nitrogen flux, the cellular structure becomes more irregular with emergence of open cell boundaries. However, composition modulation was found in all InAlN samples suggesting that elimination of the honeycomb structure cannot be achieved by simple selection of growth conditions within the previously reported growth window [1]. Our data indicates that the honeycomb structure is determined at the earliest stage of film growth. We propose that the honeycomb structure is due to delayed formation of an indium adlayer resulting in low aluminum adatom mobility at the nucleation stage.

InAlN films were grown by PAMBE on commercially available (0 0 0 1) GaN templates. Typical dislocation densities of these templates are $5 \times 10^8 \, cm^{-2}$. GaN templates were solvent-cleaned, etched with HCl, and degassed in high vacuum conditions prior to growth. The PAMBE system is equipped with conventional effusion cells for indium, aluminum, and gallium. Nitrogen was supplied by a Veeco Unibulb radio frequency plasma source. The active nitrogen flux was tuned by varying the plasma power from 250 W to 400 W, and the $N_2$ flow rate from 0.15 to 1.0 standard cubic centimeters per minute (SCCM), respectively. The active nitrogen flux was determined from high resolution x-ray diffraction (HRXRD) measurements of the thickness of GaN layers in AlGaN/GaN superlattices grown under metal rich conditions at 720 °C. The impinging metal fluxes were measured as beam equivalent pressure (BEP) and reported in terms of atomic flux (atoms/ $cm^2s$). The aluminum flux was calibrated through the thickness of InAlN layers assuming that at growth temperature $T_s < 600 \, °C$ all aluminum is preferentially incorporated [13]. The impinging indium flux was calibrated through the growth of an InN film at a substrate temperature where thermal InN decomposition and indium adatom desorption are negligible ($< 435 \, °C$). Prior to the InAlN growth, a 200 nm thick GaN buffer layer was grown at 720 °C using modulated growth under Ga-rich conditions to ensure a smooth surface. Excess gallium was either incorporated into the GaN lattice or thermally desorbed from the surface during periodic growth interruptions under nitrogen flux, and at the end of the buffer growth. After each GaN buffer layer growth, gallium consumption is monitored via full recovery of the reflection high energy electron diffraction signal intensity.

A series of InAlN layers nearly lattice-matched to GaN was grown with different nitrogen fluxes while holding the Al flux constant. For each nitrogen flux, substrate temperature and In/Al flux ratio determine indium composition. Furthermore, at fixed nitrogen flux and temperature, there is a maximum possible (saturated) indium mole fraction. Further increase of the indium flux leads to accumulation of indium on the surface, but no increase in indium composition. Therefore, for each nitrogen flux, the temperature and indium flux were selected large enough to grow $In_{0.17}Al_{0.83}N$ slightly above the border for droplet formation. Indium mole fractions were determined by analysis of HRXRD data of symmetric $\omega - 2\theta$ scans around the (0 0 0 2) GaN reflection. The surface morphology of the InAlN films was assessed

**Table 1**
Growth conditions of the nearly lattice-matched InAlN layers grown by PAMBE at the constant aluminum flux $\Phi_{Al} = 6.1 \times 10^{13}$ atoms/cm² s and saturated InN mole fraction.

| Sample # | $\Phi_N$ (atoms/ cm² s) | T (°C) | In/Al | III/V | In content, $x$ | Thickness (nm) |
|---|---|---|---|---|---|---|
| i | $1.75 \times 10^{14}$ | 506 | 0.7 | 0.59 | 0.174 | 30 |
| ii | $2.70 \times 10^{14}$ | 519 | 0.7 | 0.38 | 0.172 | 30 |
| iii | $4.23 \times 10^{14}$ | 539 | 0.9 | 0.28 | 0.154 | 29 |
| iv | $6.42 \times 10^{14}$ | 552 | 1.0 | 0.19 | 0.165 | 29 |
| v | $1.26 \times 10^{15}$ | 561 | 1.2 | 0.11 | 0.162 | 28 |

by atomic force microscopy (AFM). High-angle annular dark-field scanning transmission electron microscopy (HAADF-STEM) and energy dispersive x-ray spectroscopy (EDXS) were used to reveal the degree of indium segregation and evolution of cellular structure as a function of growth conditions. Specimens for plan-view analysis by HAADF-STEM were prepared using a standard TEM sample preparation technique [14]. The thickness of each specimen was reduced to 10–15 μm by mechanical polishing and dimpling. Then, the sample was thinned down to electron transparency using a precision ion polishing system.

To study the effect of growth conditions on indium segregation in lattice-matched InAlN, the nitrogen flux was varied from $1.75 \times 10^{14}$ to $1.26 \times 10^{15}$ atoms/cm² s. Practically, for each nitrogen flux, several InAlN films were grown at different substrate temperatures. The growth temperature was varied until the saturated indium composition of $0.17 \pm 0.01$ was achieved. The growth conditions of nearly lattice-matched InAlN/GaN structures discussed in this paper are summarized in Table 1. All growths were conducted in the nominally nitrogen-rich regime with the ratio of total metal flux to nitrogen flux $(\Phi_{Al} + \Phi_{In})/\Phi_N < 1$. Since aluminum is fully incorporated into the lattice in the temperature range 500–560 °C, the impinging aluminum flux was kept the same for all samples, $\Phi_{Al} = 6.1 \times 10^{13}$ atoms/cm² s, corresponding to an InAlN growth rate of 1 nm/min. Higher growth rates can be achieved with higher aluminum fluxes. However, a notable deterioration of material quality occurs at higher growth rates [8]. The impinging indium flux was selected for each sample to supply slightly more indium to the surface than can be both incorporated and desorbed at a given nitrogen flux and substrate temperature to ensure the saturated indium composition. The excess indium on the surface was experimentally confirmed by the presence of dilute droplets after the growth. It is known that increase of the growth temperature leads to the monotonic decrease of the indium composition in the InAlN lattice under fixed flux conditions due to thermal decomposition [15,16]. However, the growth under higher nitrogen fluxes allowed us to preserve the lattice-matched composition at elevated temperatures as discussed in the next section.

The symmetric $\omega - 2\theta$ scans around the (0 0 0 2) GaN peak of InAlN layers are shown in Fig. 1. The HRXRD spectra were analyzed assuming that the InAlN film is fully strained and coherent to the underlying GaN buffer layer. The indium content was calculated using Vegard's law specifying the InAlN lattice constants [17]. Pendellösung satellite fringes indicate that the InAlN layers possess a high degree of thickness uniformity. However, it was previously reported that the indium composition assessed by HRXRD might be underestimated by about 3–5% in comparison with the indium composition provided by atom probe tomography [1,10].

The surface morphology of the nearly lattice-matched InAlN series was characterized by Nomarski optical microscopy and AFM. Since impinging indium flux was kept slightly above the total indium incorporation and thermal desorption rates, widely-spaced indium droplets were observed on the surface of most samples upon growth termination. Indium droplets indicate that the indium composition reached its maximum value limited by substrate temperature. However, if needed, the impinging indium flux can be adjusted to achieve a
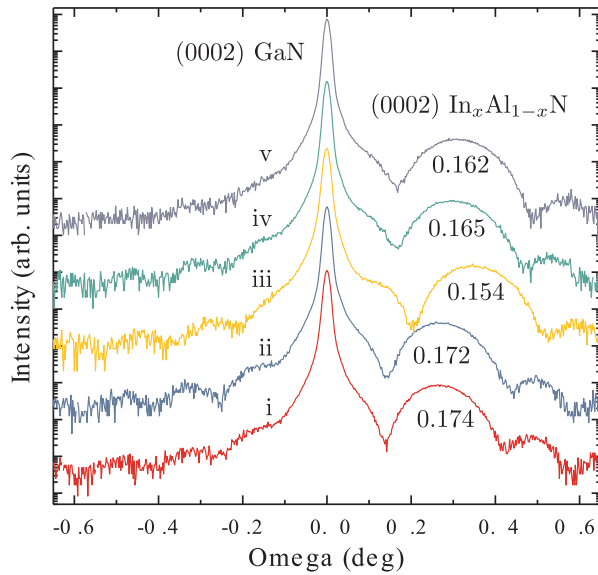
**Fig. 1.** Symmetric HRXRD $\omega-2\theta$ scans around the (0002) GaN reflection for the series of nearly-lattice-matched InAlN/GaN structures grown under different nitrogen fluxes $\Phi_N$ and correspondingly adjusted substrate temperatures: $\Phi_N$ of i – $1.75 \times 10^{14}$, ii – $2.70 \times 10^{14}$, iii – $4.23 \times 10^{14}$, iv – $6.42 \times 10^{14}$, v – $1.26 \times 10^{15}$ atoms/cm² s. The saturated indium content $x_{In}$ is limited by the growth temperature $T$ at a given nitrogen flux $\Phi_N$.



**Fig. 3.** PAMBE growth diagram for InAlN lattice-matched to GaN at the aluminum flux $\Phi_{Al} = 6.1 \times 10^{13}$ atoms/cm² s. The closed circles show the conditions used for the InAlN films i-v. At a given nitrogen flux, the substrate temperature, $T$, and the indium flux, $\Phi_{In}$, were adjusted to generate a saturated indium composition of about $x_{In} = 0.17$. The color code indicates the In/Al flux ratio for each sample. The growth parameters reported for homogeneous InAlN are indicated by the black star [1]. The solid line is given by Arrhenius dependence at the activation energy 1.92 eV [12]. Error bars are indicated; otherwise, error bars are the same size or smaller than the symbols. (For interpretation of the references to color in this figure legend, the reader is referred to the web version of this article.)

droplet-free surface without changing the InAlN alloy composition. Virtually no droplets were observed on the surface of sample v due to the efficient indium removal from the surface by a significant indium desorption at 560 °C.

Fig. 2 shows the surface morphologies of 30-nm-thick nearly-lattice matched InAlN layers (i-v) as well as a representative GaN buffer layer. Note that despite the nominally nitrogen-rich growth conditions, smooth morphology and stepped terraces are observed. For III-Nitride growth via plasma-assisted MBE, such morphology is usually associated

with growth under a metallic adlayer that promotes surface mobility. We speculate that the high indium flux and thermal decomposition of InN leads to an indium adlayer. The observed stepped terrace structure is qualitatively consistent with step-flow growth around spiral hillocks. The formation of spiral hillocks occurs due to steps pinned around screw dislocations under step-flow growth conditions [18]. All samples i-v exhibit very similar surface morphology both qualitatively and
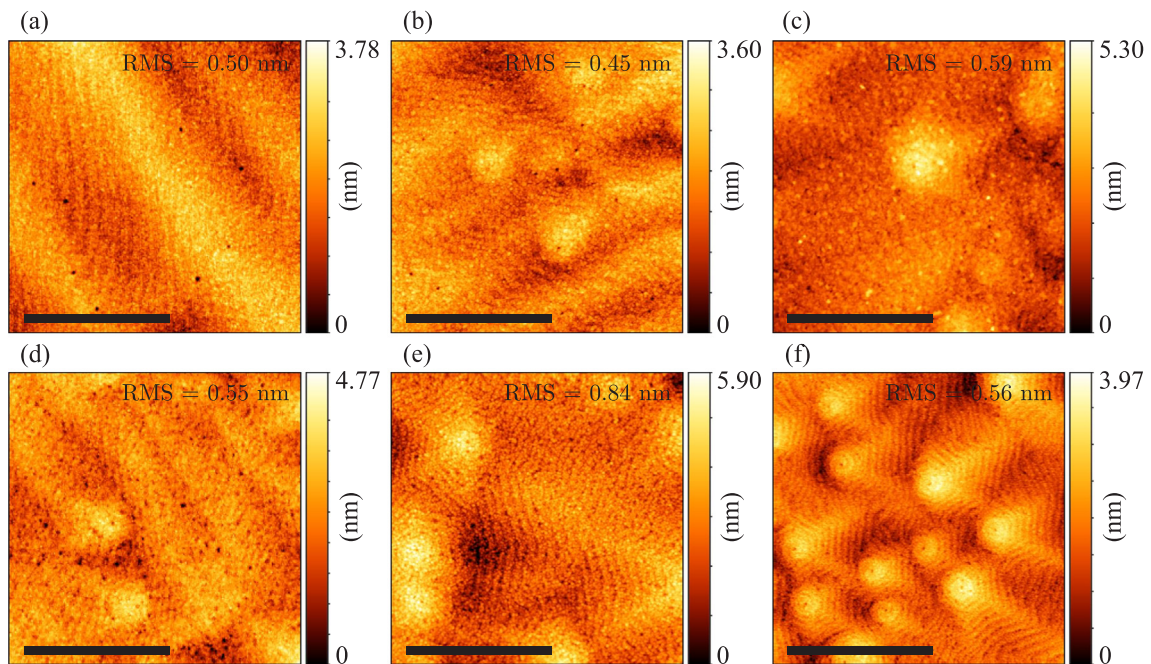


**Fig. 2.** $2 \times 2\,\mu m^2$ AFM micrographs of the surface of InAlN layers grown in this study using the nitrogen flux $\Phi_N$ of (a) i – $1.75 \times 10^{14}$, (b) ii – $2.70 \times 10^{14}$, (c) iii – $4.23 \times 10^{14}$, (d) iv – $6.42 \times 10^{14}$, (e) v – $1.26 \times 10^{15}$ atoms/cm² s. The surface morphology shows stepped terrace structure consistent with the step-flow growth around spiral hillocks. (f) GaN layer grown under the nitrogen flux $\Phi_N = 6.42 \times 10^{14}$ atoms/cm² s at the substrate temperature $T = 720$ °C for comparison. The scale bar for all micrographs is 1 µm.

quantitatively (Fig. 2). The root-mean square (RMS) roughness of all samples is comparable with that of the representative GaN buffer layer (0.56 nm), except for structure v that has slightly higher RMS roughness (0.84 nm). Since the samples in the lattice-matched InAlN series i-v show comparable indium composition and surface morphology, they are particularly interesting for comparative study of composition modulation in InAlN due to the lateral indium segregation.

Fig. 3 plots the growth conditions, i.e. active nitrogen flux and the substrate temperature, for structures i-v (see Table 1) that provide InAlN layers with the saturated indium mole fraction $x_{In} \sim 0.17$. In the growth temperature range 500–560 °C, thermally activated InN decomposition is the main physical process that limits indium solubility [16]. The actual In mole fraction in the grown film may differ substantially from the nominal mole fraction $\Phi_{In}/(\Phi_{Al} + \Phi_{In})$ predicted based on impinging metal fluxes. An increase of growth temperature leads to a monotonic decrease of the saturated indium content [15,16]. Indium that is not incorporated into the lattice accumulates on the surface or desorbs. It was found that, at a given growth temperature, an increase of the nitrogen flux increases the indium solubility limit. Therefore, the saturated indium content $x_{In} \sim 0.17$ in the lattice-matched InAlN films can be maintained by increasing the nitrogen flux as we raise the growth temperature.

The experimental data allows us to construct a complete growth diagram for the lattice-matched InAlN layers at the given aluminum flux $\Phi_{Al} = 6.1 \times 10^{13}$ atoms/cm²s. We assess the nitrogen flux necessary to yield a saturated indium mole fraction $x_{In} \sim 0.17$ as a function of substrate temperature by fitting the experimental data with an Arrhenius dependence of activation energy $E_a = 1.92$ eV governed by InN thermal decomposition [12].

We demonstrated that InAlN/GaN structures with saturated indium composition $x \sim 0.17$ can be grown over a wide range of growth conditions and constructed the growth diagram for lattice-matched InAlN layers in Fig. 3. We now turn to the impact of these conditions on compositional modulation in InAlN without the complication of significant indium composition changes from sample to sample. The degree of lateral indium segregation in our samples was assessed by plan-view HAADF-STEM imaging. The intensity of HAADF-STEM micrographs strongly depends on the atomic number (Z) of the scattering atoms, which makes this technique appropriate for composition distribution analysis. Areas of a sample comprised of atoms with a higher atomic number appear brighter on HAADF-STEM micrographs. In Fig. 4, HAADF-STEM micrographs of nearly lattice-matched InAlN layers grown in this study are shown. The plan-view HAADF-STEM images were taken along [0 0 0 1] zone axis projection. The bright regions on the micrographs represent areas with higher indium content. The lateral indium segregation generates a cellular structure with lower indium content inside the cells (dark areas) and higher indium content at the cell boundaries (bright areas).

The cellular structure in Z-contrast HAADF-STEM micrographs associated with lateral indium segregation was observed for all lattice-matched InAlN layers grown in our study. However, notable changes of the cellular structure as a function of growth conditions were found. Specifically, the size of cells in HAADF-STEM micrographs increases for samples grown at elevated temperatures and nitrogen fluxes. Moreover, the cellular structure becomes more irregular with emergence of open cell boundaries at the highest growth temperature and nitrogen flux. This data clearly indicates the impact of the growth conditions, substrate temperature and nitrogen flux, on the cellular structure.

To assess the cell size, the spatial periodicity in the cellular structures observed in HAADF-STEM micrographs was analyzed using a two-dimensional (2D) Fast Fourier Transform (FFT) analysis. The 2D FFT converts the original HAADF-STEM micrograph into a map of spatial frequency components. Insets in Fig. 4(a–d) show 2D FFT patterns of the cellular structures formed by lateral indium segregation. The color code indicates the intensity of spatial frequency components. The significant frequency components in all directions form a high intensity ring. The size of the ring represents a particular frequency that can be converted back to the spatial periodicity of the cellular structure. To estimate the size of the ring, i.e. the most significant frequency component, the 2D FFT power spectra were radially averaged to obtain the direction-independent mean 1D profile. The analysis of 2D FFT power spectra is presented in detail in the Supplemental Material (SM, Fig. S2). For example, the dominant component in the 2D FFT of the HAADF-STEM micrograph in Fig. 4(a) is $0.13 \pm 0.01$ nm$^{-1}$ and represents periodicity in the original micrograph of about $7.5 \pm 0.6$ nm, which can be used as an estimate of the average size of cells. The results of 2D FFT are summarized in Table 2.

Supplementary data associated with this article can be found, in the online version, at https://doi.org/10.1016/j.jcrysgro.2018.08.016.

Cellular, or 'honeycomb', microstructure was previously observed in several studies of lattice-matched InAlN layers grown by PAMBE [9,10,19]. Here we present a systematic study of the impact of growth conditions on compositional modulation in InAlN. While it is clear that modification of growth parameters does influence the process of indium segregation, all samples in our study display some degree of cellular structure. We recently extended our study to growth temperature 570 °C, but cellular structure is still evident. Furthermore, quantitative EDXS analysis of indium composition fluctuation across 'honeycomb' cells demonstrates that the amplitude of the indium fluctuations at the cell boundary does not change significantly with growth conditions (SM, Fig. S1). The discrepancy between our observations and those reported in Ref. [1] indicates that subtle differences at the early stages of InAlN nucleation on GaN must play a decisive role in InAlN nanostructure formation.

Theoretical calculations suggest that InAlN alloys are miscible at the indium compositions used in our study and observed compositional
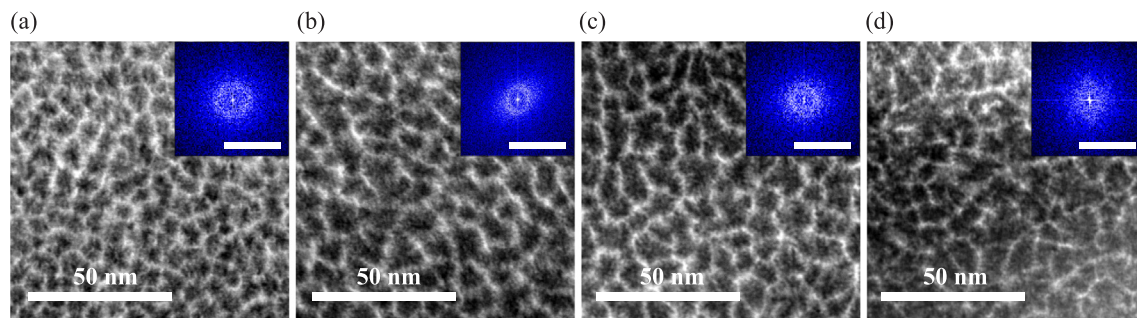


**Fig. 4.** Plan-view HAADF-STEM images taken in the [0 0 0 1] zone axis projection for InAlN films grown at the nitrogen flux of (a) i – $1.75 \times 10^{14}$, (b) iii – $4.23 \times 10^{14}$, (c) iv – $6.42 \times 10^{14}$, (d) v – $1.26 \times 10^{15}$ atoms/cm² s. The insets show the 2D discrete FFT power spectra as a function of spatial frequency for each HAADF-STEM micrograph using a color scale ranging from low (blue) to high (white) intensity. The scale bar of the insets is 0.5 nm$^{-1}$. Periodicity of a cellular structure in all directions results in a circular profile in spatial frequency. The radius of the circle represents a spatial frequency of the original periodic 2D structure. (For interpretation of the references to color in this figure legend, the reader is referred to the web version of this article.)

**Table 2**
Results of 2D FFT analysis of HAADF-STEM micrographs providing an estimate of the distance between cells.

|          | Sample i        | Sample iii      | Sample iv       | Sample v         |
|----------|-----------------|-----------------|-----------------|------------------|
| 2D FFT   | 7.5 ± 0.6 nm    | 9.8 ± 0.7 nm    | 9.7 ± 1.0 nm    | 12.1 ± 1.5 nm    |

modulation is difficult to explain by spinodal decomposition [20,21]. Moreover, examination of cross-sectional HAADF-STEM images (not shown) indicates the cellular indium segregation propagates vertically throughout the entire film forming a columnar microstructure, also not consistent with spinodal decomposition. In work by Ivanov et al. [22], the origin of composition inhomogeneity in InN and In(Ga,Al)N alloys is related to the formation of indium metal nanoparticles. Indium atoms have high surface mobility at growth temperature and can diffuse to grain boundaries, pores, or high-density exits of vertical threading dislocations [22]. Preferential incorporation of indium along these defects was found to lead to the formation of indium nanoparticle arrays extending along the growth direction and at the InN/GaN interface. However, extensive compositional analysis of our InAlN films did not reveal any metallic indium nanoparticles inside InAlN epilayers so far. Moreover, the density of defects such as threading dislocations in lattice-matched InAlN/GaN on GaN templates is significantly lower than that of the alloy composition fluctuations shown in Fig. 4. Therefore, we believe that the honeycomb microstructure is initiated by structural or compositional nonuniformities at the early stages of InAlN growth [9,19].

The indium segregation experimentally observed here can be well explained by the model that considers the growth kinetics of InAlN layers at the early stages [9]. Specifically, it is expected that the growth of InAlN on GaN is initiated by formation of dynamical aluminum-rich InAlN platelets [9,23]. Subsequent material deposition increases the size of platelets, while their coalescence leads to generation of elastic tensile strain between adjacent platelets. Indium preferentially incorporates at platelet boundaries due to this tensile strain, generating a lateral compositional gradient which then propagates throughout the entire film thickness [9]. Therefore, the honeycomb microstructure observed in HAADF-STEM micrographs of our samples (Fig. 4) is directly related to formation of InAlN platelets with indium composition increasing at the platelet boundaries.

The size of the dynamic platelets formed at the early stage reflects the metal adatom mobility on the surface. At the growth temperatures used in this work, Al atoms are fully incorporated into the lattice. Thus, the increase of the cell size observed in HAADF-STEM micrographs can be attributed to an increase of Al adatom mobility. Adatom mobility can be modified either by growth temperature or the use of a surfactant. For instance, indium can be used as a surfactant to improve aluminum adatom mobility [24]. In our experiments, the growth of InAlN was carried out under an indium adlayer. Since the impinging indium flux was larger than both indium incorporation and indium desorption rates (also evidenced by indium droplet formation), an indium adlayer is expected to be formed under steady state conditions. This indium surfactant adlayer is expected to decrease the diffusion barrier of metal adatoms and is consistent with the smooth terraced morphology of the resulting InAlN films with low RMS roughness (Fig. 2). Such morphology is not seen for nitrogen-rich GaN growth [25].

Growth under an indium adlayer should increase the aluminum adatom mobility which is expected to lead to more homogeneous InAlN growth. However, even though our samples were grown under an indium adlayer, the cellular structure was not completely eliminated. We speculate that this structure is due to the delayed formation of the indium adlayer on the surface during deposition of the first few layers. Given the modest growth temperature necessary to incorporate indium, aluminum adatoms have a short diffusion length during the earliest stages of growth, leading to a dense array of small platelets. As growth
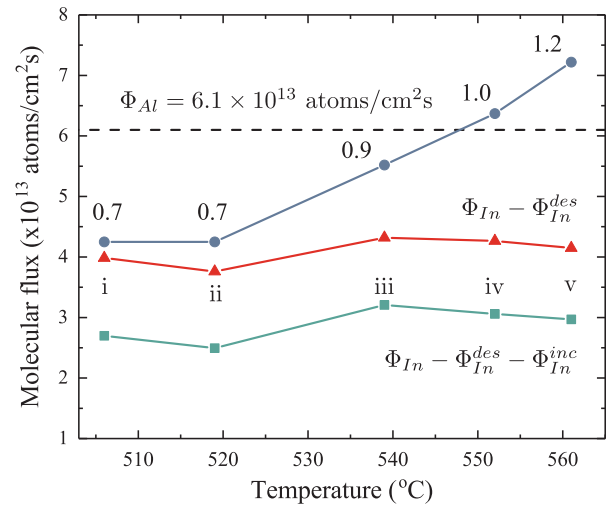


**Fig. 5.** Indium accumulation rate on the surface for samples i-v. Blue circles represent the impinging indium flux. At higher growth temperature, the indium flux was increased to compensate indium losses due to the thermal desorption $\Phi_{In}^{des}(T)$ and maintain growth under indium adlayer. The In/Al ratio is shown for each sample. Red triangles show the difference between the impinging indium flux and indium steady state desorption rate $\Phi_{In}^{des}(T)$. The green squares show the difference between the impinging indium flux, indium steady state desorption rate, and incorporation rate. (For interpretation of the references to color in this figure legend, the reader is referred to the web version of this article.)

proceeds, indium is accumulated on the surface. Once a critical indium surface coverage is reached, the aluminum adatom mobility increases and growth proceeds in step-flow mode, consistent with the smooth morphology observed in the AFM scans. Thus limited aluminum adatom mobility due to delayed formation of an indium adlayer can simultaneously explain several of our observations including the presence of cellular microstructure, the dependence of the cell size on growth temperature, and curiously enough, the smooth morphology of 30-nm-thick films indicative of step flow growth.

To preserve saturated indium composition at elevated temperatures, the indium flux has to be increased to compensate indium losses from the growth front due to thermal desorption. To assess the formation of the indium adlayer, the indium accumulation rate on the surface was calculated for samples i-v by subtracting from the impinging flux $\Phi_{In}$ the fluxes due to thermal desorption, $\Phi_{In}^{des}(T) = C^{des} \times \exp(-E_a^{des}/k_B T)$, where $E_a^{des} = 2.49$ eV and $C^{des} = 3.4 \times 10^{28}$ atoms/cm$^2$ s given in Refs. [12,26], and incorporation, $\Phi_{In}^{inc}$. The results of these calculations are plotted in Fig. 5. The impinging indium flux is shown in blue circles. The difference between impinging flux, $\Phi_{In}$, and the calculated desorption flux, $\Phi_{In}^{des}$, is shown in red triangles in Fig. 5. If we also consider indium loss from the growth front due to its incorporation into the lattice $\Phi_{In}^{inc}$ at the early stage of growth, the indium accumulation rate can be estimated as $\Phi_{In} - \Phi_{In}^{des} - \Phi_{In}^{inc}$ taking $x_{In} = 0.17$ (Fig. 5, green squares). As can be seen, the effective surface indium accumulation rate for all samples does not change dramatically, even as the In/Al ratio was increased from 0.7 to 1.2. From the data in Fig. 5 (red triangles), the required time for the formation of a 2.5 monolayer (ML) thick indium adlayer [12] is estimated to be about ∼70 s. This estimation assumes a planar atomic density $11.35 \times 10^{14}$ atoms/cm$^2$ for the GaN surface. The estimated delay of indium adlayer formation would result in a growth of about 3.8ML of AlN in the effectively nitrogen-rich regime. Therefore, we suggest that the presence of the honeycomb microstructure in our samples results from the delayed formation of an indium adlayer and growth of first layers of the material under effectively nitrogen-rich regime, even though the AFM data indicates that indium adlayer was present at later stages. Moreover, the increase of the cell size in the series cannot be explained solely by increased In/Al ratio, since the rate of indium adlayer formation was essentially the

same for all samples.

In our experiments InAlN growth is initiated in the absence of an indium adlayer. The nitrogen-rich $2 \times 2$-reconstructed GaN surface presents a high diffusion barrier for Al adatoms resulting in low Al adatom mobility, and formation of a dense network of nucleation centers. However, increased substrate temperature promotes Al adatom diffusion even under nitrogen-rich conditions and leads to the monotonic increase of the cell size with increased growth temperature observed in Fig. 4. This hypothesis is also supported by previously published results showing large InAlN platelets grown at high temperatures [9]. Therefore, the main physical mechanism leading to increase of cell size under the currently employed growth conditions is enhanced mobility of aluminum adatoms with increasing temperature. Nevertheless, over the range of growth parameters explored in this work, increases in substrate temperature were not sufficient to completely remove the cellular structure and influence compositional inhomogeneity. Therefore, rapid formation of an indium adlayer at the early stage of InAlN growth may be essential for elimination of the cellular microstructure. A systematic study of surface treatments with indium flux prior to initiation of InAlN growth will be presented in a future publication.

In conclusion, a series of InAlN layers was grown systematically varying the PAMBE growth conditions, while preserving the saturated indium mole fraction $x_{In} \sim 0.17$. We constructed a growth diagram that identifies the nitrogen flux at a given substrate temperature required to attain lattice-matched $In_xAl_{1-x}N/GaN$ structures. Electron microscopy analysis allowed us to study the impact of growth conditions on compositional modulation in nearly lattice-matched InAlN layers. We found that samples grown at higher temperatures and correspondingly increased nitrogen fluxes and In/Al ratios show a trend toward larger irregular cells often accompanied by open cell boundaries. We conclude that the growth temperature is the main factor determining the observed changes. The impact of increased In/Al ratio is rather minor due to the proportional increase of the indium desorption at elevated temperatures. Most importantly, we found that studied growth conditions, including those reported in literature as conducive to homogeneous InAlN, are not alone sufficient to eliminate the 'honeycomb' indium segregation in InAlN. We attribute the formation of the honeycomb structure in our samples to delayed formation of an indium adlayer.

## Acknowledgements

## References

[1] S.W. Kaun, E. Ahmadi, B. Mazumder, F. Wu, E.C.H. Kyle, P.G. Burke, U.K. Mishra, J.S. Speck, Semicond. Sci. Technol. 29 (2014) 045011.
[2] O. Ambacher, R. Dimitrov, M. Stutzmann, B.E. Foutz, M.J. Murphy, J.A. Smart, J.R. Shealy, N.G. Weimann, K. Chu, M. Chumbes, B. Green, A.J. Sierakowski, W.J. Schaff, L.F. Eastman, Phys. Stat. Sol. 216 (1999) 381.
[3] J.A. del Alamo, J. Joh, Microelectron. Reliab. 49 (2009) 1200.
[4] D.S. Lee, X. Gao, S. Guo, D. Kopp, P. Fay, T. Palacios, IEEE Electr. Dev. Lett. 32 (2011) 1525.
[5] H.J. Kim, S. Choi, S.-S. Kim, J.-H. Ryou, P.D. Yoder, R.D. Dupuis, A.M. Fischer, K. Sun, F.A. Ponce, Appl. Phys. Lett. 96 (2010) 101102.
[6] S. Choi, M.-H. Ji, J. Kim, H. Jin Kim, M.M. Satter, P.D. Yoder, J.-H. Ryou, R.D. Dupuis, A.M. Fischer, F.A. Ponce, Appl. Phys. Lett. 101 (2012) 161110.
[7] O. Malis, C. Edmunds, M.J. Manfra, D.L. Sivco, Appl. Phys. Lett. 94 (2009) 161111.
[8] M. Shirazi-HD, K. Turkmeneli, S. Liu, S. Dai, C. Edmunds, J. Shao, G. Gardner, D.N. Zakharov, M.J. Manfra, O. Malis, Appl. Phys. Lett. 108 (2016) 121108.
[9] S.-L. Sahonta, G.P. Dimitrakopulos, T. Kehagias, J. Kioseoglou, A. Adikimenakis, E. Iliopoulos, A. Georgakilas, H. Kirmse, W. Neumann, P. Komninou, Appl. Phys. Lett. 95 (2009) 021913.
[10] S. Choi, F. Wu, R. Shivaraman, E.C. Young, J.S. Speck, Appl. Phys. Lett. 100 (2012) 232102.
[11] C. Edmunds, L. Tang, M. Cervantes, M. Shirazi-HD, J. Shao, A. Grier, A. Valavanis, J.D. Cooper, D. Li, G. Gardner, D.N. Zakharov, Z. Ikonić, D. Indjin, P. Harrison, M.J. Manfra, O. Malis, Phys. Rev. B 88 (2013) 235306.
[12] C.S. Gallinat, G. Koblmüller, J.S. Brown, J.S. Speck, J. Appl. Phys. 102 (2007) 064907.
[13] G. Koblmueller, R. Averbeck, L. Geelhaar, H. Riechert, W. Hösler, P. Pongratz, J. Appl. Phys. 93 (2003) 9591.
[14] J. Ayache, L. Beaunier, J. Boumendil, G. Ehret, D. Laub, Sample Preparation Handbook for Transmission Electron Microscopy, Springer, New York, New York, NY, 2010.
[15] S. Fernández-Garrido, Ž. Gačević, E. Calleja, Appl. Phys. Lett. 93 (2008) 191907.
[16] R. Averbeck, H. Riechert, Phys. Stat. Sol. 176 (1999) 301.
[17] H.M. Foronda, B. Mazumder, E.C. Young, M.A. Laurent, Y. Li, S.P. DenBaars, J.S. Speck, J. Cryst. Growth 475 (2017) 127.
[18] B. Heying, E.J. Tarsa, C.R. Elsass, P. Fini, S.P. DenBaars, J.S. Speck, J. Appl. Phys. 85 (1999) 6470.
[19] L. Zhou, D.J. Smith, M.R. McCartney, D.S. Katzer, D.F. Storm, Appl. Phys. Lett. 90 (2007) 081917.
[20] V.G. Deĭbuk, A.V. Voznyi, Semiconductors 39 (2005) 623.
[21] G. Zhao, X. Xu, H. Li, H. Wei, D. Han, Z. Ji, Y. Meng, L. Wang, S. Yang, Sci. Rep. 6 (2016) 26600.
[22] S.V. Ivanov, T.V. Shubina, T.A. Komissarova, V.N. Jmerik, J. Cryst. Growth 403 (2014) 83.
[23] A. Bourret, C. Adelmann, B. Daudin, J.-L. Rouvière, G. Feuillet, G. Mula, Phys. Rev. B 63 (2001) 245307.
[24] E. Monroy, B. Daudin, E. Bellet-Amalric, N. Gogneau, D. Jalabert, F. Enjalbert, J. Brault, J. Barjon, L.S. Dang, J. Appl. Phys. 93 (2003) 1550.
[25] B. Heying, I. Smorchkova, C. Poblenz, C. Elsass, P. Fini, S. Den Baars, U. Mishra, J.S. Speck, Appl. Phys. Lett. 77 (2000) 2885.
[26] Ž. Gačević, V.J. Gómez, N.G. Lepetit, P.E.D. Soto Rodríguez, A. Bengoechea, S. Fernández-Garrido, R. Nötzel, E. Calleja, J. Cryst. Growth 364 (2013) 123.